Open access • Journal Article • DOI:10.1140/EPJA/I2009-10814-6

In-trap decay of 61Mn and Coulomb excitation of 61Mn/61Fe

J. Van de Walle, V. Bildstein, N. Bree, Joakim Cederkäll ...+20 more authors

Institutions: CERN, Technische Universität München, Katholieke Universiteit Leuven, Lund University ...+1 more institutions

Published on: 09 Jun 2009 - European Physical Journal A (Springer)

Topics: Coulomb excitation and Ion source

Eur. Phys. J. A **42**, 401–406 (2009)
DOI 10.1140/epja/i2009-10814-6

THE EUROPEAN PHYSICAL JOURNAL A

Regular Article – Experimental Physics

In-trap decay of ^{61}Mn and Coulomb excitation of ^{61}Mn/^{61}Fe

J. Van de Walle[1,a], V. Bildstein[2], N. Bree[3], J. Cederkäll[1,4], P. Delahaye[5], J. Diriken[3], A. Ekström[4], V.N. Fedosseev[5], R. Gernhäuser[2], A. Gustafsson[1], A. Herlert[1], M. Huyse[3], O. Ivanov[3], T. Kröll[2], R. Krücken[2], B. Marsh[5], N. Partronis[3], P. Van Duppen[3], D. Voulot[5], N. Warr[6], F. Wenander[5], K. Wimmer[2], and S.M. Lenzi[7]

[1] PH department, CERN, Switzerland
[2] Physik Department E12, Technische Universität München, Garching, Germany
[3] Instituut voor Kern- en Stralingsfysica, K.U. Leuven, Leuven, Belgium
[4] Lund University, Lund, Sweden
[5] AB department, CERN, Switzerland
[6] Institut für Kernphysik, Universität Köln, Köln, Germany
[7] Dipartimento di Fisica dell'Università di Padova and INFN, Padova, Italy

Received: 19 December 2008 / Revised: 15 April 2009
Published online: 9 June 2009 –
Communicated by J. Äystö

Abstract. At ISOL (Isotope Separator On-Line) facilities, which utilize thick primary production targets, beams of neutron-rich iron isotopes are difficult to obtain due to the long extraction time of these isotopes out of the target matrix. At REX-ISOLDE, an exploratory experiment was carried out to investigate the possibility of producing a post-accelerated beam of neutron-rich iron isotopes by the in-trap decay of neutron-rich manganese isotopes, which are available at ISOLDE using the Resonance Ionization Laser Ion Source (RILIS). This production mechanism was tested for the first time at REX-ISOLDE with an intense and short-lived beam of ^{61}Mn isotopes. In this work, the proof of principle of this method is demonstrated, although the technical details of the trapping process are currently not well understood and are still under investigation. The first physics results on the Coulomb excitation of ^{61}Mn and ^{61}Fe are presented and compared to shell model calculations.

PACS. 23.20.Gq Multipole mixing ratios – 25.70.De Coulomb excitation – 29.38.Gj Reaccelerated radioactive beams

1 Introduction

Iron isotopes form interesting nuclei to probe the onset of collectivity below the nickel isotopic chain ($Z < 28$) around $N = 40$. From the energy systematics of the first excited 2^+ states in iron isotopes, a decrease of the 2^+ state is apparent at $N = 38$, which is an indication for more collective behavior around $N = 40$ [1]. The calculated $B(E2)$ values of iron isotopes from ref. [2] indicate the crucial role played by the $1\nu g_{9/2}$ orbital in the apparent enhanced collective behavior in iron isotopes with $N > 36$. In order to validate the quoted and other shell model calculations in this region, new experimental information is needed. Low energy Coulomb excitation is a good tool to probe transition strengths between low-lying states, which are benchmarks to validate theoretical predictions. In this work, a Coulomb excitation study of $^{61}Mn_{36}$ and $^{61}Fe_{35}$ performed at REX-ISOLDE (CERN) is described. In sect. 2, the pioneering indirect production method of the iron beam at REX-ISOLDE is described and in sect. 3, the transition strengths in ^{61}Mn and ^{61}Fe obtained by Coulomb excitation, are presented and compared to large-scale shell model calculations.

2 In-trap decay and Coulomb excitation

At Isotope Separator On-Line (ISOL), which utilize thick primary production targets, intense beams of short-lived iron isotopes are difficult to obtain due to the long extraction time of these isotopes out of the target material matrix. In order to circumvent this intrinsic extraction problem, an alternative method to produce a post-accelerated beam of neutron-rich iron isotopes has been explored at ISOLDE. Thanks to the availability of the Resonance Ionization Laser Ion Source (RILIS) [3], intense beams of neutron-rich manganese isotopes ($Z = 25$) are available at ISOLDE [4]. These isotopes are produced by proton-induced fission of uranium, utilizing a thick UC_x target

[a] e-mail: jarno.van.de.walle@cern.ch

and 1.4 GeV proton beam from the PS Booster (CERN). The laser-ionized Mn^{1+} isotopes are extracted from the ion source with a 30 kV potential and mass separated. The 30 keV isobaric beam is subsequently bunched in a Penning trap (REXTRAP) [5] and injected in the Electron Beam Ion Source (EBIS) [6] prior to post-acceleration with the REX linear accelerator [7]. Bunching in the REXTRAP is needed to improve the beam properties to enable an efficient injection to the EBIS. The latter is needed to charge breed the isotopes from the initial charge state of 1+ to higher charge states in order to obtain an $A/q \leq 4.5$, which is the design limit of the REX linear accelerator. During the trapping and charge breeding times, which are typically 10–200 ms, the short-lived neutron-rich manganese isotopes (half-life $T_{1/2} < 1$ s for $A > 60$) undergo β^--decay into relatively long-lived iron isotopes ($T_{1/2} < 2$ s for $A < 65$). This in-trap decay can be exploited to transform a significant fraction of the trapped manganese isotopes into iron isotopes and potentially an intense post-accelerated beam of iron isotopes could be produced. At the ISOLTRAP setup at ISOLDE, a successful mass measurement of neutron-rich iron isotopes was performed in a similar way, *i.e.* by the in-trap decay of neutron-rich manganese isotopes [8]. An exploratory experiment has been carried out at REX-ISOLDE to examine the feasibility of this production mechanism using the REXTRAP and EBIS combination. One of the technical uncertainties is whether or not the energetic recoiling daughter product (typically some hundred eV) remains trapped in the REXTRAP and EBIS. Typical values for the trapping potentials are 165 V at the entrance and 230 V at the extraction side of REXTRAP and 500 V in the EBIS. A suitable candidate for this in-trap decay test was found in ^{61}Mn ($T_{1/2} = 670(40)$ ms, see fig. 1) with a primary target yield of 1.7E6 atoms/μC proton beam. The maximum recoil energy of the ^{61}Fe daughter is 475 eV. The observed β-decay spectrum in the MINIBALL germanium detector array did not give any indication for isobaric contamination from surface-ionized ^{61}Ga (half-life 150(30) ms). From a measurement in a ΔE (Gas)-$E_{\rm rest}$ (Si) detector at the end of the linear accelerator, no contamination was observed with $Z < 25$ or $Z > 26$. In the following a pure $A = 61$ beam is assumed.

In a first experiment the ^{61}Mn isotopes were continuously injected into the REXTRAP, where they were trapped for 30 ms and subsequently charge bred for 28 ms in the EBIS. The A/q separator after the EBIS was set to 4.07 ($^{61}Mn^{15+}$). The REXTRAP was not synchronized with the proton impacts at this point. Decay losses of ^{61}Mn during these trapping and charge breeding times are limited. Since the isotopes diffusing from the primary target are continuously injected in the REXTRAP, the total trapping time for the captured isotopes depends on their arrival time at the REXTRAP entrance barrier. Thus, the exponential decay is averaged over the time the isotopes are injected in the REXTRAP, which is referred to as the REXTRAP beam gate (T). This time-averaged exponential decay is given by $\frac{1}{T}\int_0^T e^{-\lambda_{\rm Mn}t}{\rm d}t$. In the EBIS, all isotopes spend the same amount of time and a straightforward exponential decay is assumed. Thus, with 30 ms trapping time and 28 ms charge breeding time, $\approx 96\%$ of the post-accelerated beam should consist of ^{61}Mn isotopes. The isotopes were post-accelerated to a final energy of 2.87 MeV A and impinged upon a 4.0 mg/cm^2 ^{109}Ag target, where Coulomb excitation was induced. The total post-accelerated beam intensity was 1.3E5 isotopes/s. The resulting Coulomb excitation spectrum, background subtracted and Doppler corrected for the detected beam particle is shown in fig. 2. Two Doppler-corrected γ-ray transitions are identified at 157 keV and 878 keV, which de-excite the $(7/2^-)$ and $(9/2^-)$ state in ^{61}Mn, respectively (see fig. 1). The low-lying excited states in ^{61}Mn, which were recently published in [9], are confirmed with the current Coulomb excitation experiment. Spin assignments from the same reference are adopted and are consistent with the non-observation of any de-excitation γ-rays from the $(11/2^-)$ level, which cannot be excited from the $(5/2^-)$ ground state by the dominating single-step $E2$ excitation probability in low-energy Coulomb excitation. Both the 157 keV and 878 keV transitions can have a mixed

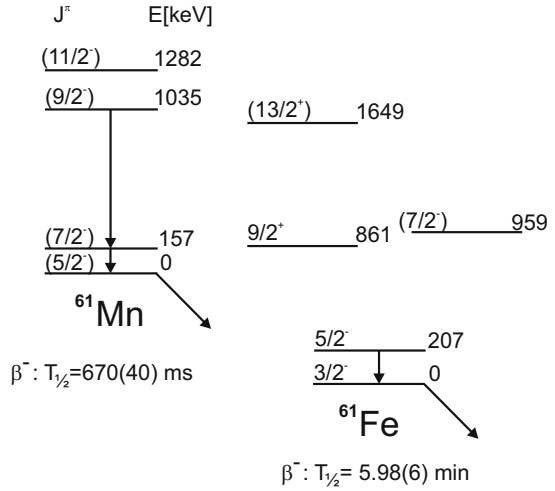

Fig. 1. Level schemes of ^{61}Mn and ^{61}Fe. Data is taken from [9–11].

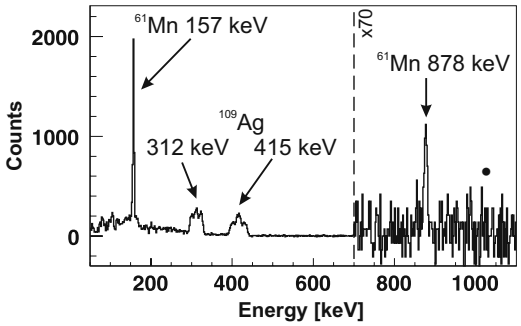

Fig. 2. The Coulomb excitation spectrum obtained with 28 ms charge breeding time and 30 ms trapping time. The spectrum is Doppler corrected for the detected projectile particle and random subtracted. The filled circle indicates the non-observed Doppler-corrected $(9/2^-) \rightarrow (5/2^-_{\rm g.s.})$ transition at 1035 keV.

$E2/M1$ character, whereas the non-observed 1035 keV de-excitation from the $(9/2^-)$ state to the $(5/2^-)$ ground state has a pure $E2$ nature. Furthermore, strong γ-ray transitions are observed at 312 keV and 415 keV (smeared out in the spectrum due to the Doppler correction), corresponding to known transitions in the target nucleus ^{109}Ag.

The amount of target excitation induced by ^{61}Mn is given by

$$N^{\mathrm{Mn}}_{\gamma,\mathrm{Ag}} = N^{\mathrm{Total}}_{\gamma,\mathrm{Ag}} \Big/ \left(1 + \frac{1-\alpha}{\alpha} \cdot \frac{\sigma^{\mathrm{Fe}}_{\mathrm{Ag}}}{\sigma^{\mathrm{Mn}}_{\mathrm{Ag}}}\right), \qquad (1)$$

where α is the fraction of ^{61}Mn isotopes in the beam, σ_{Ag} is the cross-section for ^{109}Ag excitation by either ^{61}Mn or ^{61}Fe and $N^{\mathrm{Mn,Total}}_{\gamma,\mathrm{Ag}}$ is the number of counts in the Ag de-excitation line (induced by Mn or the full beam). From this, the ratio of the 157 keV (^{61}Mn de-excitation) and 312 keV (^{109}Ag de-excitation, induced by ^{61}Mn) γ-ray intensities, can be established:

$$N_{\gamma,157\,\mathrm{keV}}/N^{\mathrm{Mn}}_{\gamma,\mathrm{Ag}} = 1.25(4). \qquad (2)$$

This ratio will be used as a reference to identify any change in the ^{61}Mn content of the beam.

A first attempt to increase the ^{61}Fe content in the post-accelerated beam was made by trapping the ^{61}Mn^{1+} ions over longer time periods in the REXTRAP, ranging from 200 to 1100 ms. The breeding time in the EBIS was fixed to 28 ms. Since the charge breeding time was not changed, the A/q separator after the EBIS was set again to 4.07 (^{61}Mn^{15+}). The REXTRAP was synchronized with the proton beam impact and a beam gate of 200 ms was applied to the incoming isotopes, reducing the post-accelerated beam intensity to 5.0×10^3 isotopes/s. This synchronization implies that all produced ^{61}Mn isotopes which are released up to 200 ms after the proton impact are trapped and charge bred for the same amount of time (except for the small difference due to the different arrival times of the isotopes at the TRAP barrier, see above), resulting in a constant Fe/Mn ratio in the post-accelerated beam pulse from the EBIS. The proton pulses are separated by a minimum of 1.2 s, thus the maximum trapping plus charge breeding time is limited to this value. The resulting Coulomb excitation spectrum, which is the sum of all spectra acquired with different trapping times, is shown in fig. 3(A).

The target de-excitation lines at 312 keV and 415 keV are clearly identified together with the Doppler-corrected line at 157 keV. No evidence is found for a Doppler-corrected 207 keV γ-ray, which is expected from the known level scheme of ^{61}Fe (fig. 1). From the observed amount of 157 keV γ-rays and the ratio from eq. (2), 68(10) counts are expected in the 312 keV transition for 96% ^{61}Mn in the beam. Experimentally, a total of 76(10) γ-rays are observed. Thus, no evidence is found for a strong ^{61}Fe component in the post-accelerated beam. A straightforward calculation, using the exponential decay of ^{61}Mn during the trapping and charge breeding times (a time-weighted average of the trapping times was taken), results in a total of 61% of ^{61}Mn in the beam.

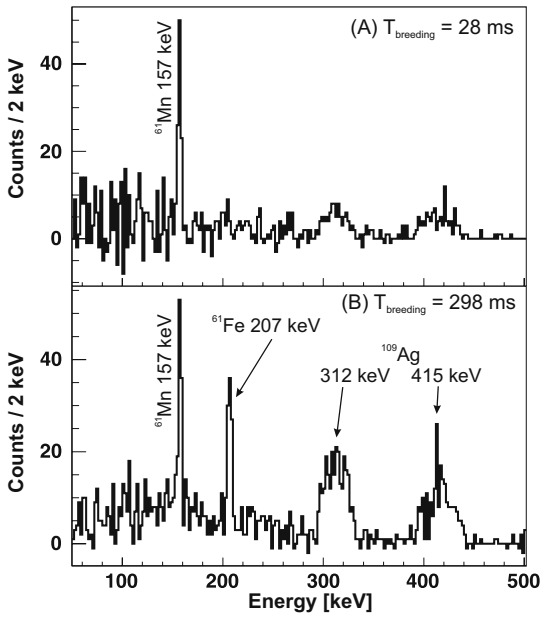

Fig. 3. The sum of all Coulomb excitation spectra obtained with 28 ms (A) and 298 ms (B) charge breeding time and with variable trapping times, ranging from 200 up to 1100 ms (A) and from 300 up to 900 ms (B). The spectrum is Doppler corrected for the detected projectile particle and random subtracted.

In a second trial to increase the ^{61}Fe content, the trapping times were varied from 300 to 900 ms and the breeding time was increased and fixed to 298 ms. Because of this longer charge breeding time, the A/q separator after the EBIS was set to 2.9 (^{61}Mn^{21+}). The REXTRAP was synchronized again with the proton beam and a beam gate of 300 ms was applied to the extracted ^{61}Mn^{1+} ions, effectively reducing the post-accelerated beam intensity to 1.0×10^4 isotopes/s. The resulting Coulomb excitation spectrum, which is the sum off all different trapping times, is shown in fig. 3(B). In this case, a de-excitation γ-ray is observed at 207 keV, which is the $5/2^- \rightarrow 3/2^-_{\mathrm{g.s.}}$ transition in ^{61}Fe. Utilizing the factor from eq. (2) and subtracting the resulting target excitation induced by ^{61}Mn from the total amount of target excitation observed, a total manganese content of 39(6)% is deduced. A total of 49% manganese content is expected using the exponential decay, described above.

The reason for the large discrepancy between the calculated manganese content and the experimental observation in the first experiment (charge breeding time = 28 ms) is not well understood. It is clear that a straightforward exponential decay inside the REXTRAP and EBIS neglects possible losses of ^{61}Fe after the β-decay of ^{61}Mn, due to the recoil energy and/or the n^+ ($n \geq 2$) charge state of ^{61}Fe. These possible losses might be induced by the insufficient cooling of ^{61}Fe^{n+} in the REXTRAP and thus the poor injection into the EBIS, poorly known recombination times for ^{61}Fe^{n+}, the possible difference in charge state distributions of Fe and Mn after charge breeding, charge exchange with the buffer gas atoms, collisions of

Table 1. Transition rates resulting from the Coulomb excitation study of ^{61}Mn and ^{61}Fe. Constraints on the values indicated with $(*)$ can be read from fig. 5(B). $(**)$ Experimentally, the g.s. spin is found to be $3/2^-$.

$J_i \to J_f$	$E(J_i \to J_f)$ [keV]			$B(E2, J_i \to J_f)$ [W.u.]			$B(M1, J_i \to J_f)$ [W.u.]		
	Exp	GXPF1A	pfg	Exp	GXPF1A	pfg	Exp	GXPF1A	pfg
				^{61}Mn					
$(7/2^-) \to (5/2^-)$	157	152	161	30(4)	20	27	$(*)$	0.040	0.011
$(9/2^-) \to (7/2^-)$	878	1072	847	$(*)$	6.9	1.7	$(*)$	0.021	0.009
$(9/2^-) \to (5/2^-)$	1035	1224	1008	$(*)$	6.4	7.7	–	–	–
				^{61}Fe					
$(3/2^-) \to (1/2^-)$	$(**)$	290	130	–	–	–	–	–	–
$(5/2^-) \to (3/2^-)$	207	195	308	17(7)	14.4	14.2	$(*)$	0.025	0.034

the recoiling ^{61}Fe with the walls and electrodes inside the trap, and so on. These topics are of high interest and are currently being investigated at REX-ISOLDE. The current data can serve as valuable input to establish simulation tools which model the decay processes and kinematics inside REXTRAP.

3 Results and discussion

The transition strength between the ground state and first excited state in ^{61}Mn and ^{61}Fe can be deduced from the normalization to the known target excitation. The γ-ray intensities were integrated in the spectra shown in fig. 2 (157 keV, ^{61}Mn $(7/2^-) \to (5/2^-_{\text{g.s.}})$) and in fig. 3(B) (207 keV, ^{61}Fe $5/2^- \to 3/2^-_{\text{g.s.}}$). The Coulomb excitation code GOSIA [12] was used to calculate the de-excitation yields from both the target and projectile nuclei. GOSIA takes into account the energy loss of scattered beam and recoiling target particles in the target, the internal conversion coefficients for all γ-ray transitions (taken from [13]) and performs the integration of the cross-section over the laboratory scattering angles. Matrix elements for the target nucleus ^{109}Ag were deduced from $B(E2)$ and $B(M1)$ values taken from [14].

In a first approach, only the ground state and first excited states in ^{61}Mn and ^{61}Fe were considered. The $E2/M1$ mixing ratio for the $(7/2^-) \to (5/2^-_{\text{g.s.}})$ and $5/2^- \to 3/2^-_{\text{g.s.}}$ transitions in ^{61}Mn and ^{61}Fe (respectively) could not be deduced from the angular distribution of the γ-rays in MINIBALL due to lacking statistics in each individual germanium detector. Therefore, the $E2$ matrix element between the ground state and first excited state was fitted (to reproduce the calculated ratio of projectile and target excitation to the experimental ratio) for a fixed value of the $M1$ matrix element, varying from $0\,\mu_N$ to $0.5\,\mu_N$. In fig. 4 the resulting partial half-life of the $(7/2^-)$, $5/2^-$ state in ^{61}Mn, ^{61}Fe (respectively) is given as a function of the $M1$ matrix element. For each partial half-life, two lines are drawn which indicate the error on the $E2$ matrix element, given by the statistical error on the number of counts in the 157 keV and 207 keV transitions for ^{61}Mn and ^{61}Fe (respectively) and the error on the target matrix elements. Since both transitions are observed with a Doppler shift, the partial half-life of the $(7/2^-)$ and $5/2^-$ states is lower than the minimum flight time between the secondary target and the particle detector, which is 1.7 ns. This condition constrains the $M1$ matrix elements, as can be seen from fig. 4. The resulting $B(E2)$ values for these two transitions are given in table 1 for $M1$ matrix elements of $0.25\,\mu_N$ ($B(M1) = 0.008\,\mu_N^2$ for ^{61}Mn) and $0.14\,\mu_N$ ($B(M1) = 0.003\,\mu_N^2$ for ^{61}Fe). The $B(E2)$ values in table 1 decrease by $\approx 0.9\%$ and 0.4% for ^{61}Mn and ^{61}Fe, respectively, when the $M1$ matrix elements are increased from $0.25\,\mu_N$ ($0.14\,\mu_N$) to $0.5\,\mu_N$. The error on the $B(E2, 7/2^- \to 5/2^-_{\text{g.s.}})$ value for ^{61}Mn, quoted in table 1 includes as well the influence of higher-lying states on the resulting $B(E2)$ value, as described below.

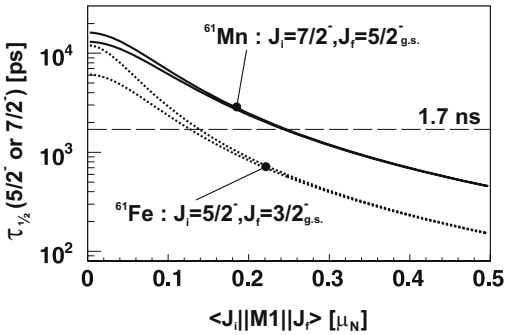

Fig. 4. Resulting partial half-lives for the $(7/2^-)$ and $5/2^-$ states in ^{61}Mn and ^{61}Fe, respectively, as a function of the $M1$ matrix element connecting these states to the ground states. The two lines for both partial half-lives indicate the statistical error (see text).

To investigate the influence of the higher-lying states on the $(7/2^-) \to (5/2^-_{\text{g.s.}})$ yield in ^{61}Mn, the $(9/2^-)$ state at 1035 keV was included as well in the calculation. This introduces two additional $E2$ matrix elements connecting the $(9/2^-)$ state with the $(5/2^-_{\text{g.s.}})$ and $(7/2^-)$ states and one $M1$ matrix element connecting the $(9/2^-)$ and $(7/2^-)$ state. Two experimental observations can be used to fit these additional three matrix elements. One is the relative intensity of the 878 keV γ-ray intensity compared to the 157 keV transition and the second is the non-observation of the $(9/2^-) \to (5/2^-_{\text{g.s.}})$ E2 transition at 1035 keV.

The value of the $\langle 5/2^-_{\text{g.s.}} || M1 || 7/2^- \rangle$ matrix element was fixed to $0.25\,\mu_N$, based on the half-life considera-

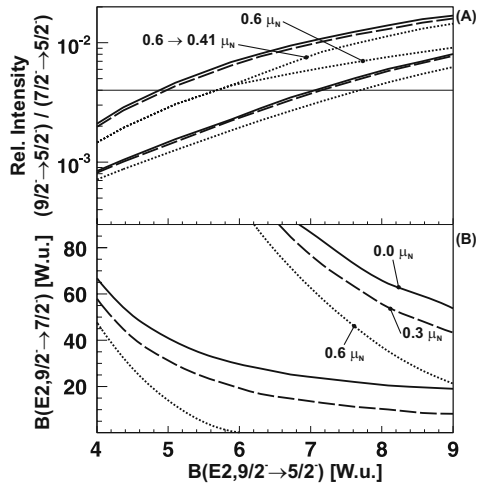

Fig. 5. Results from the fitting of the matrix elements to the experimental data: (A) calculated relative intensity of the $(9/2^-) \rightarrow (5/2^-_{\rm g.s.})$ to the $(7/2^-) \rightarrow (5/2^-_{\rm g.s.})$ transition in ^{61}Mn as a function of the $E2$ matrix element connecting the $(9/2^-)$ and $(5/2^-_{\rm g.s.})$ ground state. Full, dashed and dotted lines correspond to a fixed $\langle 9/2^- || M1 || 7/2^- \rangle$ of 0.0, 0.3 and $0.6\,\mu_N$, respectively (see text for details). (B) The resulting $B(E2, 9/2^- \rightarrow 7/2^-)$ and $B(E2, 9/2^- \rightarrow 5/2^-_{\rm g.s.})$ as a function of each other and $\langle 9/2^- || M1 || 7/2^- \rangle$. The values in between the parallel lines (full, dotted and dashed) are consistent with the experimental observations, taking into account the statistical error on the relative intensity of the 878 keV transition.

tions mentioned above. The $\langle 9/2^- || M1 || 7/2^- \rangle$ matrix element was fixed to $0.0\,\mu_N$, $0.3\,\mu_N$ and $0.6\,\mu_N$ in three fitting procedures and the results are summarized in fig. 5. In fig. 5(A) the resulting intensity of the non-observed $(9/2^-) \rightarrow (5/2^-)$ transition, relative to the $(7/2^-) \rightarrow (5/2^-)$ transition, is shown. The full, dotted and dashed lines correspond to three different $M1$ matrix elements (see above). The full horizontal line corresponds to a 0.4% relative intensity for the 1035 keV γ-ray, which would correspond to 15 counts in the Doppler-corrected spectrum of fig. 2 (indicated with a dot). Figure 5(B) shows the resulting $B(E2)$ values as a function of each other (on the axes) and the $\langle 9/2^- || M1 || 7/2^- \rangle$ matrix element (in the figure itself). The two parallel lines (full, dotted and dashed) in each of these plots indicate the upper and lower limit on the $B(E2)$ values, given by the statistical error on the observed relative intensity of the 878 keV γ-ray transition. The inclusion of the $(9/2^-)$ state in the calculation of γ-ray yields, changes the resulting $B(E2, 7/2^- \rightarrow 5/2^-_{\rm g.s.})$ value, obtained above (*i.e.* without the $9/2^-$ included), by $\pm 3.5\%$. As mentioned above, this change was incorporated in the final error bar quoted in table 1.

From fig. 5(B) it is clear that the $B(E2, 9/2^- \rightarrow 7/2^-)$ and $B(E2, 9/2^- \rightarrow 5/2^-_{\rm g.s.})$ values strongly depend on the $M1$ matrix element between the $(9/2^-)$ state and the $(7/2^-)$ state. These three matrix elements determine the de-excitation properties of the $(9/2^-)$ state. In the lower limit of the $B(E2, 9/2^- \rightarrow 7/2^-)$ value, with its associated $M1$ matrix element $= 0.6\,\mu_N$, the observed $(9/2^-) \rightarrow (7/2^-)$ relative intensity can be accounted for by a pure $M1$ transition, thus the $(9/2^-)$ state would be populated mainly by a one-step $E2$ excitation from the ground state. The corresponding relative intensity of the 1035 keV transition for a fixed $M1$ matrix element of $0.6\,\mu_N$ (the upper dotted curve in fig. 5(A), marked $0.6\,\mu_N$) displays a discontinuity due to the vanishing $B(E2, 9/2^- \rightarrow 7/2^-)$ matrix element. Though, the relative intensity of the 878 keV transition remains within the experimental error bars for $B(E2, 9/2^- \rightarrow 7/2^-) = 0$ W.u. and 6.0 W.u. $< B(E2, 9/2^- \rightarrow 5/2^-_{\rm g.s.}) <$ 9.0 W.u. When the lower experimental limit on the relative intensity of the 878 keV transition is maintained, the $M1$ matrix element has to be lowered from $0.6\,\mu_N$ to $0.41\,\mu_N$ with $B(E2, 9/2^- \rightarrow 7/2^-) = 0$ W.u. The relative intensity of the $(9/2^-) \rightarrow (5/2^-_{\rm g.s.})$ transition for these lower $M1$ matrix elements is shown in fig. 5(A) with the upper dotted curve marked $0.6 \rightarrow 0.41\,\mu_N$.

To quantitatively understand the magnitude of the $B(E2)$ and $B(M1)$ values obtained in ^{61}Mn and ^{61}Fe, large-scale shell model calculations were performed using the ANTOINE code [15] and two different residual interactions (GXPF1A [16] and pfg [17]). The first interaction (GXPF1A), which is a modified version of the largely tested and documented GXPF1 interaction [18], includes the pf orbitals below $N = 40$ and was described in [16]. The second interaction (pfg) includes the $1\nu g_{9/2}$ orbital and has been proven to be more accurate closer to $N = 40$ [17], where the inclusion of the $\nu 1g_{9/2}$ in the valence space is crucial. In this case a core of ^{48}Ca is used and in the calculations some truncations had to be applied for the excitation of neutrons from the fp orbitals in the $\nu 1g_{9/2}$ orbital and protons from the $\pi 1f_{7/2}$ to the rest of the fp orbitals. In particular, a total of 5 nucleons (protons plus neutrons) were allowed to be promoted. The results of the two shell model calculations are summarized in table 1. Standard effective charges of $e_\pi = 1.5e$ and $e_\nu = 0.5e$ were used to calculate the $B(E2)$ values and free g-factors were used for the $B(M1)$ values. As can be seen from table 1, the position of the first excited $7/2^-$ state in ^{61}Mn is calculated accurately by both interactions, whereas the calculated position of the $9/2^-$ state differs by ≈ 200 keV. As was pointed out in [9], the average occupation number of the $\nu 1g_{9/2}$ orbital is not negligible for the $9/2^-$ state in the pfg calculations, which hints the importance of this orbital in the valence space.

The newly obtained transition strength in ^{61}Mn forms a sensitive test for both residual interactions, since it is more sensitive to the specific components in the nuclear wave functions, compared to the energy level. From table 1 it can be seen that the calculated $B(E2, 7/2^- \rightarrow 5/2^-)$ strength obtained with the pfg interaction, is closer to the new experimental value of 30(4) W.u. This indicates that already at $N = 36$ (^{61}Mn) the $\nu 1g_{9/2}$ orbital contributes to the quadrupole collectivity, even at low excitation energy.

When comparing the calculated $B(E2, 9/2^- \rightarrow 7/2^-)$ and $B(E2, 9/2^- \rightarrow 5/2^-)$ values, the major difference is

the strong reduction of the $B(E2, 9/2^- \rightarrow 7/2^-)$ and $B(M1, 9/2^- \rightarrow 7/2^-)$ strengths with the pfg interaction. Within the experimental errors on the transition strengths, no strong conclusions can be drawn (see fig. 5). Though, when comparing the order of magnitude of the theoretical $B(E2)$ values ($B(E2, 9/2^- \rightarrow 7/2^-) < 7\,\mathrm{W.u.}$ and $6.4\,\mathrm{W.u.} \leq B(E2, 9/2^- \rightarrow 5/2^-_{\mathrm{g.s.}}) \leq 7.7\,\mathrm{W.u.}$), one could conclude that $B(M1, 9/2^- \rightarrow 7/2^-)$ should be larger than 0.005 W.u. ($\langle 9/2^- || M1 || 7/2^- \rangle < 0.3\,\mu_N$), which would bring the calculated $B(E2)$ values within the experimental findings.

In the case of ^{61}Fe, both calculations predict a $1/2^-$ state as the g.s. with the $3/2^-$ at 290 keV excitation energy for the GXPF1A interaction and at 130 keV for the pfg model space. This is in disagreement with the $3/2^-$ assignment from experimental studies [19,20] and deserves further investigation. Nevertheless, the calculated energy and $B(E2)$ strength for the $5/2^- \rightarrow 3/2^-$ transition are well reproduced by both interactions, though the experimental error of the measured $B(E2)$ value is rather large (40%).

4 Conclusion

With this pioneering experiment at REX-ISOLDE it was shown that post-accelerated beams of isotopes produced by in-trap decay can be obtained and Coulomb excitation can be induced on these isotopes. This opens up possibilities to perform Coulomb excitation studies on short-lived isotopes which were previously unavailable at the ISOLDE facility due to the long extraction times from the primary target container. The unexplained losses which occur in the REXTRAP are still under investigation.

The obtained transition strengths in ^{61}Mn and ^{61}Fe compare well to large-scale shell model calculations and the need to include the $\nu 1g_{9/2}$ orbital in the valence space was pointed out, since it affects the quadrupole collectivity even at low excitation energy. It is clear that the information on transition strengths brings in an additional sensitive probe to test residual interactions.

This work was supported by FWO-Vlaanderen (Belgium), GOA/2004/03 (BOF-K.U.Leuven), the "Interuniversity Attraction Poles Programme - Belgian State - Belgian Science Policy" (BriX network P6/23) and the European Union Sixth Framework through RII3-EURONS (Contract No. 506065).

References

1. M. Hannawald *et al.*, Phys. Rev. Lett. **82**, 1391 (1999).
2. E. Caurier *et al.*, Eur. Phys. J. A **15**, 145 (2002).
3. V.N. Fedoseyev *et al.*, Nucl. Instrum. Methods B **126**, 88 (1997).
4. U. Köster *et al.*, Spectrochim. Acta. B **58**, 1047 (2003).
5. F. Ames *et al.*, Nucl. Instrum. Methods A **538**, 17 (2005).
6. F. Wenander *et al.*, Nucl. Phys. A **701**, 528 (2002).
7. O. Kester *et al.*, Nucl. Instrum. Methods B **204**, 20 (2003).
8. A. Herlert *et al.*, to be published in Eur. Phys. J. A.
9. J.J. Valiente-Dobón *et al.*, Phys. Rev. C **78**, 024302 (2008).
10. S. Lunardi *et al.*, Phys. Rev. C **76**, 034303 (2007).
11. E. Runte *et al.*, Nucl. Phys. A **441**, 237 (1985).
12. D. Cline *et al.*, Annu. Rev. Nucl. Part. Sci. **36**, 683 (1986).
13. I.M. Band *et al.*, At. Data Nucl. Data Tables **81**, 1 (2002).
14. `http://www.nndc.bnl.gov/nndc/nudat/`.
15. E. Caurier *et al.*, Acta Phys. Pol. B **30**, 705 (1999).
16. M. Honma *et al.*, Eur. Phys. J. A **23**, 499 (2005).
17. O. Sorlin *et al.*, Phys. Rev. Lett. **88**, 092501 (2002).
18. M. Honma *et al.*, Phys. Rev. C **69**, 034335 (2004).
19. M.R. Bhat, Nucl. Data Sheets **88**, 417 (1999).
20. I. Matea *et al.*, Phys. Rev. Lett. **93**, 142503 (2004).